

Model predictions for HERA, LHC and cosmic rays

A. Bunyatyan, A. Cooper-Sarkar, C. Diaconu, R. Engel, C. Kiesling, K. Kutak, S. Ostapchenko, T. Pierog, T.C. Rogers, M.I. Strikman, T. Sako

1 Hadron production

Min-bias model comparison The simple approach of section [1] allows us to extract the main observables which lead the air shower development, namely:

- cross section
- multiplicity
- forward spectra (inelasticity)
- (anti)baryon production

We will compare the commonly used hadronic interaction models for air shower simulations at HERA and LHC energies for these observables.

Hadronic interaction models There are several hadronic interaction models commonly used to simulate air showers. For high energy interactions ($E_{\text{lab}} \gtrsim 100$ GeV), the models studied here are EPOS 1.6 [2, 3], QGSJET 01 [4], QGSJET II [5, 6], and SIBYLL 2.1 [7–9]. The physics models and assumptions are discussed in, for example, [10]. All the high-energy interaction models reproduce accelerator data reasonably well but predict different extrapolations above $E_{\text{cms}} \sim 1.8$ TeV ($E_{\text{lab}} \sim 10^{15}$ eV) that lead to very different results at high energy [11, 12]. The situation is different at low energy where several measurements from fixed target experiments are available [13]. There one of the main problems is the extrapolation of measurements to the very forward phase space region close to the beam direction and the lack of measurements of pion-induced interactions. Both HERA and LHC can help to constrain these models.

Cross section As seen a previous section, the cross section is very important for the development of air showers and in particular for the depth of shower maximum. As a consequence, the number of electromagnetic particles at ground is strongly correlated to this observable (if the shower maximum is closer to ground, the number of particle is higher).

The proton-proton scattering total cross section is usually used as an input to fix basic parameters in all hadronic interaction models (see paragraph on total cross section below). Therefore, as shown Fig. 1 lefthand-side, the p - p total cross section is very well described by all the models at low energy, where data exists. And then it diverges above 2 TeV center-of-mass (cms) energy because of different model assumption. Thanks to the TOTEM experiment, the cross section will be measured accurately at LHC energy allowing a strong reduction of the model uncertainty ($\sim 20\%$). In all the figures of this subsection EPOS 1.6 is represented by a full (blue) line, QGSJET II by a dashed (red) line, QGSJET 01 by a dash-dotted (black) line and SIBYLL 2.1 by a dotted (green) line.

From p - p to proton-air interactions, the Glauber model is used in all models but with different input parameters depending on nuclear effects (none in SIBYLL 2.1, strong in QGSJET II).

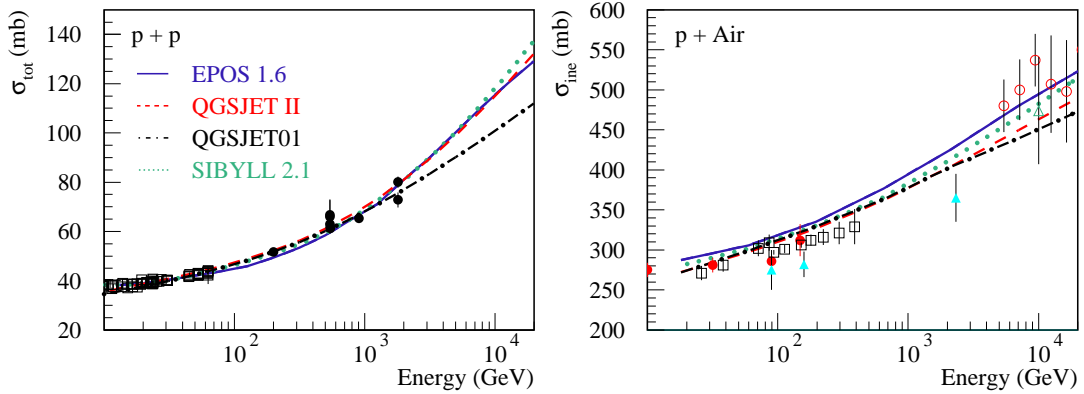


Fig. 1: Total cross section of p - p collision (lefthand-side) and inelastic proton-air cross section (righthand-side) as calculated with EPOS 1.6 (full line), QGSJET II (dashed line), QGSJET 01 (dash-dotted line) and SIBYLL 2.1 (dotted line). Points are data from accelerator [14] and cosmic ray experiment [15].

So comparing the models to each other (Fig. 1 righthand-side), differences appear even at low energy where the p - p cross section are similar. And at high energy the spread is again larger. Furthermore, the simulated cross sections seem all to increase faster than the measured one, even at low energy (< 1 TeV) where direct measurement of single hadrons from cosmic rays can be done at ground [15] (almost accelerator like measurement since proton flux is known). Proton-Carbon interactions at LHC would be very helpful to solve this problem.

Multiplicity According to Sec. [1], the multiplicity plays a similar kind of role as the cross section, but with a weaker dependence (log). On the other hand, the predictions from the models have much larger differences. As shown Fig. 2, going from the multiplicity of charged particles with $|\eta| < 3$ for nondiffractive collisions at 900 GeV cms energy (lefthand-side), where models agree with the UA5 data [16], to the multiplicity of charged particles (minimum bias) at 14 TeV (LHC) (righthand-side), the discrepancy can be larger than a factor of 2 in the tail of the distribution (and the shape is different). The EPOS model predicts much smaller multiplicity than QGSJET II.

The multiplicity distribution of charged particles is a very good test of the fundamental property of the hadronic interaction models and it should be one of the first result of the LHC experiments.

Forward spectra Forward particle distributions are crucial for air shower development because most of the energy is carried by these particles (and not the ones in the central region). The forward spectra have been measured in fixed target experiment at energies of few hundreds of GeV (few tens of GeV in cms energy) and the models reproduce this data correctly since they are used to fix some model parameters.

At higher energy, hadron collider experiments could not measure particles in the very

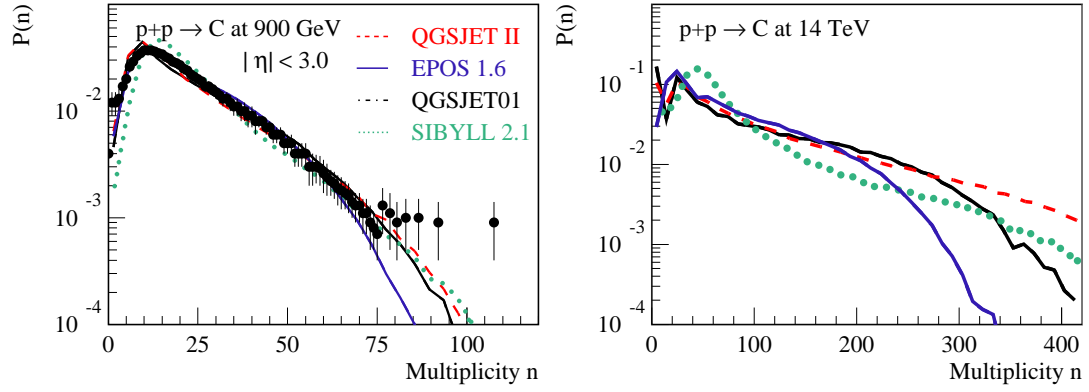


Fig. 2: Multiplicity distribution of \bar{p} - p collision at 900 GeV cms energy (lefthand-side) and 14 TeV (righthand-side) as calculated with EPOS 1.6 (full line), QGSJET II (dashed line), QGSJET 01 (dash-dotted line) and SIBYLL 2.1 (dotted line). Points are data [16].

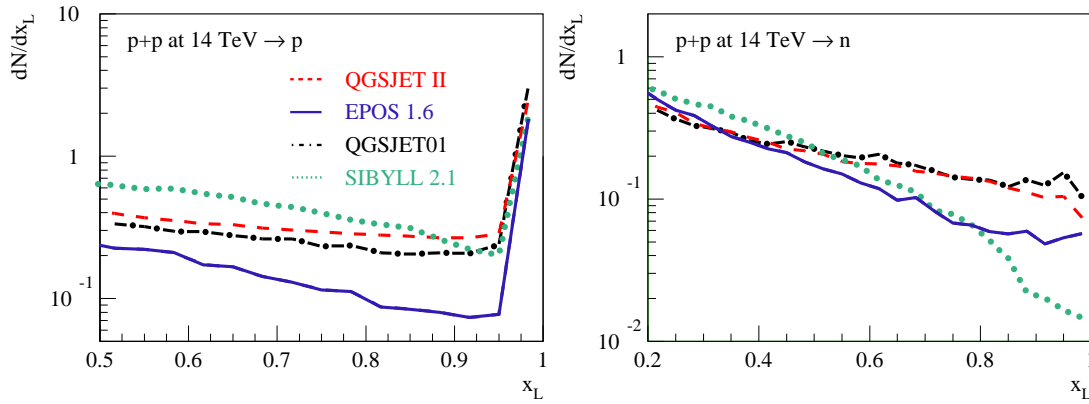


Fig. 3: Longitudinal $x_L = p_L/P_{Beam}$ distribution from p - p collision at 14 TeV cms energy for proton (lefthand-side) and neutron (righthand-side) as calculated with EPOS 1.6 (full line), QGSJET II (dashed line), QGSJET 01 (dash-dotted line) and SIBYLL 2.1 (dotted line).

forward region. But we can test the models thanks to the electron-proton HERA collider where proton or neutron production on the proton side can be measured up to very high longitudinal momentum. Results are shown Fig. [17]. While the models agree on x_L distributions at low energy, we can observe differences between them at HERA energy and in particular for EPOS 1.6 which seems to have a too strong proton dissociation in the forward region compared to the ZEUS experiment [18].

Various experiments at LHC (cf sec. [19]) should provide very usefull new data in this kinematic region, where we can see on Fig. 3, that the discrepancy between the models is very large.

(Anti)Baryon production In the forward region, the number of (anti)baryons is very important for the number of muons produced in air shower. The process is well described in [20], where it is also shown that the number of antiprotons on the projectile side of π -carbon collision can only be reproduced correctly by the EPOS model. This is due to a more sophisticated remnant treatment in this model which allows baryon number transfer from the inner part of the collision to the forward (or backward) region.

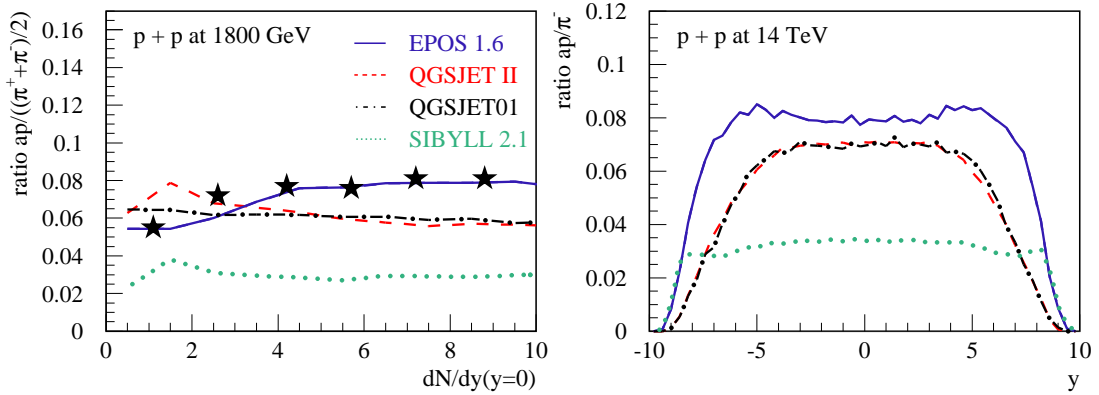


Fig. 4: Ratio of anti-proton over pion in \bar{p} - p scattering at 1.8 TeV cms energy as a function of the plateau height (lefthand-side) and rapidity distribution of this ratio for p - p interactions at LHC as calculated with EPOS 1.6 (full line), QGSJET II (dashed line), QGSJET 01 (dash-dotted line) and SIBYLL 2.1 (dotted line). Points are data [21, 22].

Another particularity of the (anti)baryons is that their production increase faster with the energy that the pion production. In other words, the ratio \bar{p}/π increase with energy. At the highest measured energy (TEVATRON [22]), we can see on the lefthand-side of Fig. 4, that only EPOS describes correctly this ratio as a function of the event multiplicity. Other models are too low.

Extrapolating to LHC, the difference between the models appears clearly on the rapidity distribution of the \bar{p}/π^- as shown Fig. 4 on the righthand-side. This ratio at midrapidity seems to saturate since the values at LHC are similar to the ones at TEVATRON, but the shape is really different comparing the models. Because of its remnant structure, EPOS predicts much more antiproton in the forward region of non-diffractive events ($|y| \sim 7$).

This explain why air showers simulated with EPOS contain more muons. Measurement of (anti)-baryon distributions at LHC will be very important to constrain muon number in air showers.

Total cross section Among the most important quantities relevant for hadronic model applications to cosmic ray (CR) physics is the total hadron-hadron cross section σ^{tot} . The reason for that is twofold. First of all, the knowledge of the total cross section implies the knowledge of the corresponding elastic scattering amplitude, taken the optical theorem relation between the two quantities. Hence, one is able to calculate the corresponding inelastic cross section and, using the Glauber formalism, to generalize these results to hadron-nucleus collisions. In turn, inelastic hadron-air cross sections are crucial quantities for the description of CR-induced nuclear-electromagnetic cascades in the atmosphere, so-called extensive air showers (EAS).

Secondly, with the total cross section being the sum of partial contributions of all possible final states for a given reaction, optical theorem allows one, within a particular model approach, to establish a correspondence between various contributions to the elastic scattering amplitude and partial probabilities of particular configurations of the interaction. Thus, available experimental information on the energy dependence of σ_{pp}^{tot} may significantly constrain model predictions for basic characteristics of hadron production in the high energy asymptotics.

In particular, such a mapping is provided by the Gribov's Reggeon Field Theory (RFT) [23], where elastic hadron-hadron scattering is described by multiple exchanges of composite objects – Pomerons. Correspondingly, inelastic cross section may be obtained as a sum of contributions of certain unitarity cuts of elastic scattering diagrams, applying the Abramovskii-Gribov-Kancheli (AGK) cutting rules [24]. There, partial contributions to $\sigma_{ad}^{\text{inel}}$ correspond to configurations of the interaction with a given number of 'elementary' production processes, the latter being described as 'cut Pomerons'. In fact, the essence of the AGK rules is that there is no interference between final states with different numbers of 'cut Pomerons', thanks to the fact that they occupy different regions of the phase space.

The described scheme takes an especially simple form if one assumes eikonal vertices for Pomeron-hadron coupling. However, one has to take into consideration contributions of multi-particle intermediate states for the projectile and target hadrons, 'between' Pomeron exchanges. The latter give rise to the diffraction dissociation and inelastic screening, the two phenomena being closely related to each other. Restricting oneself with low mass intermediate states only, one can develop a scheme of Good-Walker type, considering Pomeron-hadron coupling to be a matrix, whose elements correspond to transitions between hadronic elastic scattering eigenstates, and to obtain for total and absorptive (non-diffractive) hadron a - hadron d cross sections [25]

$$\sigma_{ad}^{\text{tot}}(s) = 2 \sum_{i,j} C_{i/a} C_{j/d} \int d^2b \left(1 - e^{-\lambda_{i/a} \lambda_{j/d} \chi_{ad}^{\text{P}}(s,b)} \right) \quad (1)$$

$$\sigma_{ad}^{\text{abs}}(s) = \sum_{i,j} C_{i/a} C_{j/d} \int d^2b \left(1 - e^{-2 \lambda_{i/a} \lambda_{j/d} \chi_{ad}^{\text{P}}(s,b)} \right) \quad , \quad (2)$$

where the Pomeron exchange eikonal $\chi_{ad}^{\text{P}}(s, b)$ is the imaginary part of the corresponding amplitude in the impact parameter representation (the small real part can be neglected in high energy

asymptotics) and $C_{i/a}$, $\lambda_{i/a}$ are relative weights and relative strengths of elastic scattering eigenstates for hadron a .

Apart from the very possibility of introducing diffraction dissociation, the above-described treatment has two important differences from the purely eikonal scheme. First, both total and inelastic cross sections are reduced, the effect being enhanced for a scattering on a nuclear target. Predictions of cosmic ray interaction models for $\sigma_{h\text{-air}}^{\text{inel}}$ sizably differ, depending on whether or not the inelastic screening corrections are taken into account and being in contradiction with available data in the latter case, see Fig. 1. Secondly and even more importantly, one obtains significantly bigger fluctuations of multiplicity of produced particles and of numbers of 'wounded' nucleons in hadron-nucleus and nucleus-nucleus interactions, which has a strong impact on specifying the 'centrality' of nuclear collisions in collider applications. It is worth stressing, however, that the described quasi-eikonal scheme can not treat high mass multi-particle intermediate states which give rise to high mass diffraction processes and result in additional screening contributions. The solution of the problem is provided by taking into consideration so-called enhanced diagrams corresponding to Pomeron-Pomeron interactions [5, 26, 27].

In hadronic interaction models, the Pomeron eikonal χ_{ad}^{P} is usually split into two parts, corresponding to partial contributions of 'soft' and 'semi-hard' parton cascades to elementary scattering process [4, 28]:

$$\chi_{ad}^{\text{P}}(s, b) = \chi_{ad}^{\text{soft}}(s, b) + \chi_{ad}^{\text{sh}}(s, b) \quad (3)$$

In particular, in the 'mini-jet' approach [28] the 'semi-hard' eikonal is expressed as the product of the corresponding inclusive cross section $\sigma_{ad}^{\text{jet}}(s, p_{t,\text{cut}})$ for the production of parton jets with transverse momentum exceeding some cutoff $p_{t,\text{cut}}$ and the hadron overlap function $A(b)$ (convolution of hadronic form factors):

$$\chi_{ad}^{\text{mini-jet}}(s, b) = \sigma_{ad}^{\text{jet}}(s, p_{t,\text{cut}}) A(b), \quad (4)$$

where the inclusive jet cross section is given by a convolution of parton distribution functions (PDFs) $f_{i/a}(x, Q^2)$ with the parton scatter cross section $d\sigma_{ij}^{2\rightarrow 2}/dp_t^2$:

$$\sigma_{ad}^{\text{jet}}(s, p_{t,\text{cut}}) = \sum_{i,j} \int dx^+ dx^- dp_t^2 f_{i/a}(x^+, p_t^2) f_{j/d}(x^-, p_t^2) \frac{d\sigma_{ij}^{2\rightarrow 2}}{dp_t^2} \Theta(p_t^2 - p_{t,\text{cut}}^2) \quad (5)$$

However, when realistic PDFs are employed, the steep energy rise of σ_{pp}^{jet} leads to a contradiction between the predicted and measured σ_{pp}^{tot} . To overcome the problem, one usually assumes that the low- x rise of hadronic PDFs is strongly damped by parton saturation effects which are often mimicked via using an energy-dependent p_t -cutoff: $p_{t,\text{cut}} = p_{t,\text{cut}}(s)$ [29]. Recently, one attempted to derive constraints on the required $p_{t,\text{cut}}(s)$ dependence, based on the ansatz (4) [30]. Nevertheless, the situation remains puzzling: on one hand, one needs significant saturation effects in order to damp the quick energy rise of σ_{pp}^{tot} , on the other – no such a strong saturation has been observed in DIS experiments at HERA. A possible solution is that the factorization ansatz (4) for the semi-hard eikonal becomes invalid when non-linear corrections to parton dynamics are taken into account [6]. The latter is easy to understand when bearing in mind that the QCD

factorization applies to fully inclusive quantities only, an example being the inclusive jet cross section (5), while being inapplicable for calculations of hadronic cross sections and of partial probabilities of particular final states. As was shown in [6], the semi-hard eikonal still can be cast in the form similar to (4-5), however, with the usual PDFs $f_{i/a}(x, Q^2)$ being replaced by reaction-dependent ones. Unlike the usual PDFs measured in DIS, those describe parton evolution *during the interaction process*, which is thus influenced by parton re-scattering on the partner hadron, as depicted in Fig. 5.

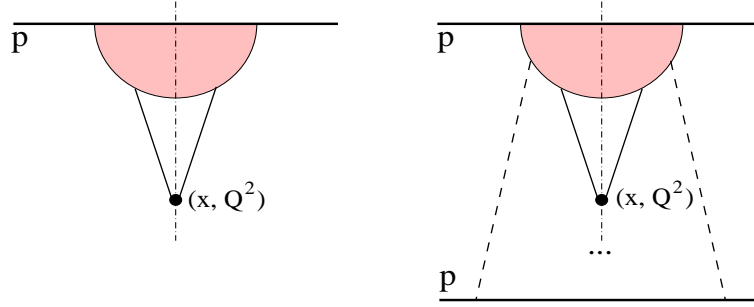


Fig. 5: Schematic view of parton distributions as “seen” in DIS (left) and in proton-proton collision (right). Low x parton (sea quark or gluon) originates from the initial state “blob” and interacts with a highly virtual “probe”. In proton-proton interaction the initial “blob” itself is affected by the collision process – due to additional soft re-scatterings on the target, indicated by dashed lines.

Screening and saturation effects in MC models Crucial differences between present hadronic MC generators are related to how they treat nonlinear interaction effects emerging in the high parton density regime. The latter appear naturally when considering hadron-hadron and, especially, nucleus-nucleus scattering in the limit of high energies and small impact parameters, where a large number of parton cascades develops in parallel, being closely packed in the interaction volume. In the QCD framework, the corresponding dynamics is described as merging of parton ladders, leading to the saturation picture: at a given virtuality scale the parton density can not exceed a certain value; going to smaller momentum fractions x , further parton branching is compensated by merging of parton cascades [31]. Importantly, at smaller x , the saturation is reached at higher and higher virtuality scale $Q_{\text{sat}}^2(x)$. The approach has been further developed in the large N_c -based color glass condensate (CGC) framework, where detailed predictions for the $Q_{\text{sat}}^2(x)$ behavior have been derived [32].

In MC generators, one usually attempts to mimic the saturation picture in a phenomenological way. Standard method, employed, e.g., in the SIBYLL model [7–9], is to treat the virtuality cutoff Q_0^2 between soft and semihard parton processes as an effective energy-dependent saturation scale: $Q_0^2 = Q_{\text{sat}}^2(s)$ and to neglect parton (and hadron) production at $|q^2| < Q_0^2(s)$. The parameters of the corresponding $Q_0^2(s)$ parametrization are usually tuned together with the other model parameters by fitting the measured proton-proton cross section.

A more sophisticated procedure has been applied in the EPOS model [3], where effective

saturation effects, being described by a set of parameters, depend on energy, impact parameter, types of interacting hadrons (nuclei). The corresponding mechanism influences not only the configuration of the interaction (how many processes of what type occur) but also the energy partition between multiple scattering processes and the hadronization procedure, the relevant parameters being fitted both with cross section and with particle production data.

An alternative approach has been employed in the QGSJET II model [5, 6], providing a microscopic treatment of nonlinear effects in the RFT framework: describing the latter by means of enhanced diagrams [26], corresponding to Pomeron-Pomeron interactions. In particular, the procedure proposed in [5] allowed one to resum contributions of dominant enhanced graphs to the scattering amplitude to all orders in the triple-Pomeron coupling. Furthermore, to treat secondary particle production, the unitarity cuts of the corresponding diagrams have been analyzed and a procedure has been worked out to resum the corresponding contributions for any particular final state of interest [27], which allowed one to implement the algorithm in the MC generator and to sample various configurations of the interaction in an iterative fashion. The main drawback of the approach is the underlying assumption that Pomeron-Pomeron coupling is dominated by soft ($|q^2| < Q_0^2$) parton processes. Thus, in contrast to the perturbative CGC treatment, the model has no dynamical evolution of the saturation scale: the saturation may only be reached at the Q_0^2 scale; at $|q^2| > Q_0^2$ parton evolution is described by purely linear DGLAP formalism.

Fragmentation of hadrons at ultra high energies Currently practically no experimental information is available on production of leading hadrons ($x_F \geq 0.1$) in the hadron - hadron collisions at the collider energies. At fixed target energies production of leading hadrons involves several partons of the projectile. For example, production of baryons in $x_F \geq 0.4$ predominantly involves at least two valence quarks of the proton, which did not experience a significant inelastic interaction, leading to a rather flat distribution in x_F . Similarly, the spectrum of the leading pions is much harder than the one corresponding to the fragmentation of one quark of the proton.

At high energies a novel situation emerges since a parton of the projectile with a given x_{pr} can resolve partons in the target with smaller and smaller $x_T \geq 4k_t^2/(x_{pr}s_{NN})$. Here k_t is typical parton transverse momentum in the interaction. The cross section of inelastic interaction is proportional to the gluon density at $x = x_T$, $Q^2 \sim 4k_t^2$. For $x_{pr} = 0.3$, $k_t = 1$ GeV/c at LHC (GZK) energies x down to $\sim 10^{-7}$ (10^{-10}) are resolved. As a result, probability of inelastic interaction for a parton passing at a fixed distance ρ from the center of the other nucleon grows with energy roughly as s^n , $n \geq 0.25$ until it reaches values close to one - the black disk regime (BDR). For example, at LHC energies, at $\rho = 1$ fm the interaction is black for the leading quarks with $p_t^2 \leq 1$ (GeV/c)² and for leading gluons with $p_t^2 \leq 2$ (GeV/c)², see [33] for the review. Between LHC and GZK energies the strength of interaction for fixed ρ , and given virtuality is expected to increase by at least a factor of five extending further the region of ρ where interaction remains black up to large virtualities. The range of ρ where interaction is black grows as a power of energy, while soft diffusion changes the radius of strong interaction logarithmically. Hence the fraction of peripheral inelastic collisions in which leading partons of the nucleon remain spectators should decrease with energy. (Obviously the effect is even stronger for the cosmic ray interactions with air ($\langle A \rangle \sim 14$).

In the BDR two effects modify fragmentation. One is that interaction selects configura-

tions in the colliding hadrons with large transverse momenta comparable to the scale of the BDR for given x_{pr}, ρ . This effectively results in the fractional energy losses [34, 35]. The second effect is the loss of coherence between the leading partons as they receive large transverse momenta and cannot fragment jointly to the same leading hadron. As a result, the projectile becomes “shattered”: The leading partons with $x \sim 0.2$ fragment independently into minijets with transverse momenta of few GeV and rapidities

$$y_{\text{minijet}} = y_{\text{max}} + \ln x - \ln(p_{\text{t BDR}}/m_N), \quad (6)$$

where $y_{\text{max}} = \ln(p_N/m_N)$. Production of hadrons from these minijets proceeds independently over a range of rapidities determined by condition that transverse momentum of hadrons in the jets due to primordial transverse momentum of a parton is larger than the soft transverse momentum scale $p_{\text{t soft}} \sim 0.4$ GeV/c. In the fragmentation process the transverse momentum of the primary parton is shared by produced partons in proportion of their light cone fractions. Hence, one can estimate the range of fractions, z , of the jet momentum where fragmentation of partons can be treated as independent:

$$z = p_{\text{t soft}}/p_{\text{t BDR}}. \quad (7)$$

For $p_{\text{t BDR}} \sim 1$ GeV/c and $x \sim 0.2 \div 0.25$ this corresponds to $x_F \geq 0.1$. With increase of energy the range where independent fragmentation is valid should expand.

In the central $p(\pi)A$ collisions where nucleus edge effects can be neglected the differential multiplicity of leading hadrons, integrated over p_{\perp} , is approximately given by the convolution of the nucleon parton density, f_a , with the corresponding parton fragmentation function, $D_{h/a}$, at the scale $Q_{\text{eff}}^2 = 4p_{\text{t BDR}}^2$ [34, 36–38]:

$$\frac{1}{N} \left(\frac{dN}{dx_F} \right)^{p+A \rightarrow h+X} = \sum_{a=q,g} \int_{x_F}^1 dx x f_a(x, Q_{\text{eff}}^2) D_{h/a}(x_F/x, Q_{\text{eff}}^2), \quad (8)$$

where N is total number of inelastic events. Eq.8 leads to a much steeper decrease of the forward spectrum with x_F than the one observed in soft collisions, and, in particular, to the π/N ratio $\gg 1$ for $x_F \geq 0.2$. Hence the large x_F inclusive spectrum is likely to be dominated by very peripheral collisions which constitute progressively smaller fraction of the collisions with increase of energy. Hence one expects that the forward multiplicity will decrease with energy. Another manifestation of this mechanism is broadening of the transverse distribution of the forward hadrons which essentially reflects transverse momenta of the forward jets [36].

First studies of these effects for GZK energies were performed in [36]. It was found that a strong increase of the gluon densities at small x leads to a steeper x_F -distribution of leading hadrons as compared to low energy collisions and results in a significant reduction of the position of the shower maximum, X_{max} . Account of this effect in the models currently used for the interpretation of the data may shift fits of the composition of the cosmic ray spectrum near the GZK cutoff towards lighter elements.

In the near future it will be possible to test experimentally these prediction in the central deuteron - gold collisions at RHIC. Another possibility is to study pp collisions at the LHC with special centrality triggers [39]. At the same time such measurements would not test dynamics

of fragmentation in ultra high-energy pion - nucleus collisions which constitute the bulk of the air showers. The interaction which is most similar to πA interactions (especially for low p_t) and could be studied at the collider energies in ultraperipheral heavy ion collisions is γA collisions. In such collisions nuclei collide at large impact parameters where one nucleus effectively serves as a source of the Weizsacker-Williams photons. At the LHC one can probe a wide range of energies $W_{\gamma N} \leq 1$ TeV [40]. For $W_{\gamma N} \leq 200$ GeV it will be possible to compare forward spectra to the HERA data on the γp collisions. It will be also possible to study forward spectrum as a function of $W_{\gamma N}$.

2 Ultra-high energy photons and s-channel unitarity

Photon cross sections at ultra-high energies Extrapolations of γp and γA cross sections to extremely high energies are frequently used in studies of ultra-high energy (UHE) cosmic rays. In particular, the UHE photon cross section is related to the cosmic ray air shower maximum, X_{max} (see [41] and references therein for a recent review). Furthermore, the identity of the primary particle affects the shape of the resulting air-shower.

At UHE energies, the incident photon interacts with the hadron target by first fluctuating into a virtual hadronic state a large distance ahead of the target. Probability of such interaction may become comparable to the probability of the electromagnetic interactions in the media, see review in [42]. Each of the virtual hadronic states interacts with the target with a strength characterized by its transverse size (which is inversely related to the state's virtuality). As the center-of-mass energy increases, there is an increasingly large contribution to the photon wavefunction from very small size quark-antiquark pairs.

It can be argued on the basis of general assumptions that the asymptotic energy dependence of photon cross sections is a power of $\ln s$ somewhere between 2 and 3 [43, 44]. An important point is that one cannot directly apply the Froissart bound, $\sigma_{tot} \sim \sigma_{\pi N} \propto \ln^2 s$, to photon-hadron interactions because the incident photon wavefunction is non-normalizable – there is an ultra-violet divergent contribution coming from small size configurations. Furthermore, a model based on the combined contributions of a hard Pomeron and a soft Pomeron [45] badly violates unitarity in the asymptotic limit because of the power-law behavior of the cross section. (This is true even if eikonalization is used to enforce s -channel unitarity, because the power-law growth of the basic cross section leads to a power-law growth of the radius of the interaction in impact parameter space.) See [46] and references therein for a review of the different types of energy dependence for the γp cross section predicted from various models.

Constraints on the growth of the photon cross section can be obtained by enforcing s -channel unitarity in impact parameter space for each individual hadronic state in the photon wavefunction. The method that we focus on here is the one used in [47] to address the unitarity limit in HERA data, and extended to the UHE real photon case in [43]. In this approach, the large size configurations have cross sections that grow at a rate typical of hadron-hadron interactions, while small size configurations have cross sections that grow according to leading twist (LT) pQCD. Intermediate sizes are obtained by extrapolating between these two regions. Configurations that grow according to LT pQCD quickly become too large to be realistic and violate s -channel unitarity. The approach in [43] is simply to allow this rapid growth, but to cut off

impact parameter dependent cross sections at their maximum possible values when they start to violate unitarity. The advantage of this approach is that it provides a conservative upper bound on the γp cross section. The main disadvantage is that it does not address the details of the higher-twist dynamical effects and/or non-perturbative effects that tame the cross section and are ultimately responsible for enforcing unitarity.

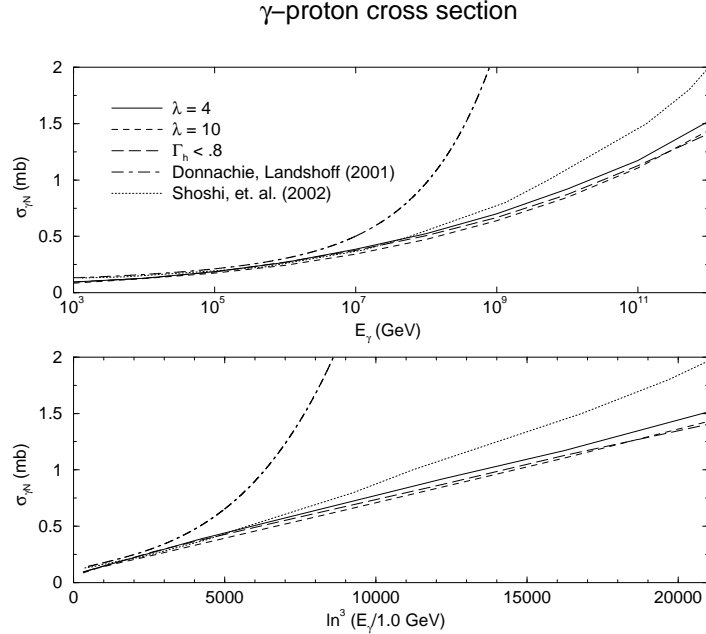


Fig. 6: The solid line is the dependence obtained the lower dashed lines show the sensitivity to variations in model parameters.

Figure 6 is taken from [43] and compares the unitarity-corrected model with models that allow a violation of s -channel unitarity. It should also be noted that the model of [43] is consistent with other extrapolations (see, e.g., [48]) based on logarithmic energy growth. Note that, although the unitarity corrections in [43] provide a conservative amount of taming, it still leads to a cross section that is less than what is predicted from parameterizations that use a power-law behavior for the basic cross section.

Charm contribution The framework in the previous section also allows for an estimate of the contribution to the photon cross section from charmed mesons.

The contribution of charm in the photon wavefunction is generally suppressed by the mass of the charm quark. However, at extremely high energies, there are large contributions from highly virtual quark-antiquark fluctuations, and for these fluctuations the suppression from the charm mass becomes negligible. If the energy is high enough that the γp cross section is entirely dominated by these very small quark-antiquark pairs, then we expect a full recovery of flavor SU(4) symmetry. In other words, we could expect up to 40% of the cross section to be due to charm quarks. An analysis of this type was performed in [43] and shows that a significant contribution, around 25% of the cross section, is due to charm quarks. See also recent work in [49].

The enhancement of the charm production in the fragmentation region in the high gluon density regime should occur also for the hadron induced cascades. It should lead to an enhancement of the production of ultra-high energy muons in the cores of air showers with energies comparable with the GZK cutoff.

Nuclear targets For γA interactions, a natural expectation is that one can directly extend the analysis for the proton target discussed in the previous section to the nuclear case by replacing the impact parameter dependent parton distribution function of the proton with the corresponding distribution function for a nucleus. However, allowing the full disk of the nuclear target to grow black yields cross sections that are even larger than what one expects from a naive extension of a Glauber type model of photon-nucleus cross sections. In a more realistic treatment, therefore, we can simply use the γp cross section from section 2 in a Glauber-Gribov treatment of the interaction with a nuclear target. A large value of the $\sigma_{diff}^{\gamma N}/\sigma_{tot}^{\gamma N} \sim 1/2$ results in a large nuclear shadowing and hence slower increase of the $\gamma - A$ cross section with energy than in the γp case. The resulting cross section from [43] is shown in Fig. 7.

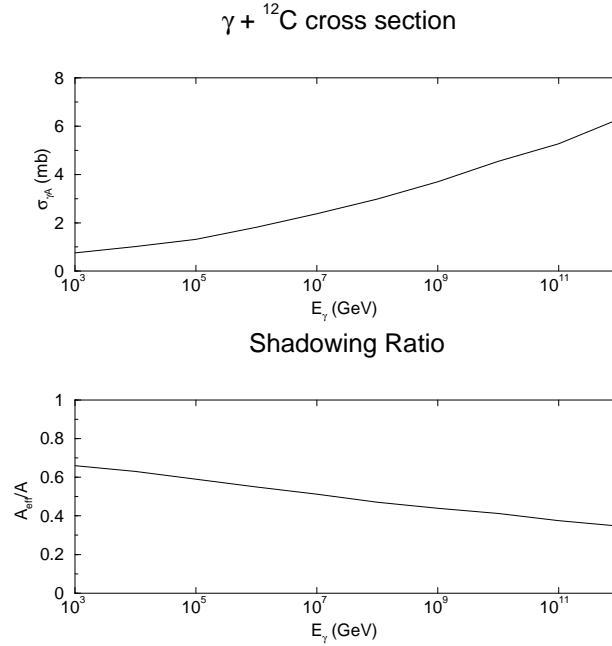


Fig. 7: The upper plot shows the cross section for a photon to scatter off Carbon using the basic cross section from section (2). The lower plot shows the corresponding shadowing ratio.

3 Extrapolation of neutrino cross section

Extrapolation of neutrino cross-section towards very high energy is needed if we want to estimate flux of ultrahigh energy neutrinos of extragalactic sources like Active Galactic Nuclei. Such estimation might be useful for Ice Cube experiment which can detect neutrinos of energy 10^{12} GeV and higher. The dominant interaction with matter at such energies is Deep Inelastic Scattering on

nucleons and in particular with the gluonic component. This gluonic system is probed roughly at $x = 10^{-8}$. In order to be consistent with unitarity bound which states that total cross-section should grow not faster than $\log^2 1/x$ one has to allow for gluon recombination effects which reduce the rate of growth of gluon density. The most suitable approach to calculate the UHE neutrino nucleon cross-section is the k_t factorisation approach (high energy factorisation). Within this scheme in order to calculate the neutrino cross-section one performs convolution of transverse momentum dependent hard matrix element (which in this case is weak boson-gluon fusion) with unintegrated gluon distribution which takes into account high energy effects. The evolution equation which introduces a large part of recombination effects in lepton-nucleon scattering is the Balitsky-Kovchegov [50] equation. This equation generalizes the BFKL [51] equation. It consists of a linear term which accounts for fast growth of gluon density at moderate values of x and nonlinear term which comes with negative sign which tames the growth of gluon density at low x . In reference [52] the calculation of $F_2(x, Q^2)^{CC,NC}$ using the BK equation (with sub-leading corrections) was performed and the UHE neutrino-nucleon cross-section was calculated. This calculation shows (see Fig. 8 (right)) that nonlinear effects reduce cross-section roughly by a factor of two as compared to approach based on linear evolution equation (BFKL with subleading corrections). In the calculation it was assumed that gluons are uniformly distributed in the nucleon. A more realistic initial distribution would increase slightly the cross section as compared to obtained from uniformly distributed gluons.

References

- [1] A. Bunyatyan et al, *Introduction*. These proceedings.
- [2] H. J. Drescher, M. Hladik, S. Ostapchenko, T. Pierog, and K. Werner, Phys. Rept. **350**, 93 (2001), arXiv:hep-ph/0007198.
- [3] K. Werner, F.-M. Liu, and T. Pierog, Phys. Rev. **C74**, 044902 (2006), arXiv:hep-ph/0506232.
- [4] N. N. Kalmykov, S. S. Ostapchenko, and A. I. Pavlov, Nucl. Phys. Proc. Suppl. **52B**, 17 (1997).
- [5] S. Ostapchenko, Phys. Lett. **B636**, 40 (2006), arXiv:hep-ph/0602139.
- [6] S. Ostapchenko, Phys. Rev. **D74**, 014026 (2006), arXiv:hep-ph/0505259.
- [7] R. S. Fletcher, T. K. Gaisser, P. Lipari, and T. Stanev, Phys. Rev. **D50**, 5710 (1994).
- [8] J. Engel, T. K. Gaisser, T. Stanev, and P. Lipari, Phys. Rev. **D46**, 5013 (1992).
- [9] R. Engel, T. K. Gaisser, T. Stanev, and P. Lipari. Prepared for 26th International Cosmic Ray Conference (ICRC 99), Salt Lake City, Utah, 17-25 Aug 1999.
- [10] S. Ostapchenko, Czech. J. Phys. **56**, A149 (2006), arXiv:hep-ph/0601230.
- [11] J. Knapp, D. Heck, S. J. Sciutto, M. T. Dova, and M. Risse, Astropart. Phys. **19**, 77 (2003), arXiv:astro-ph/0206414.

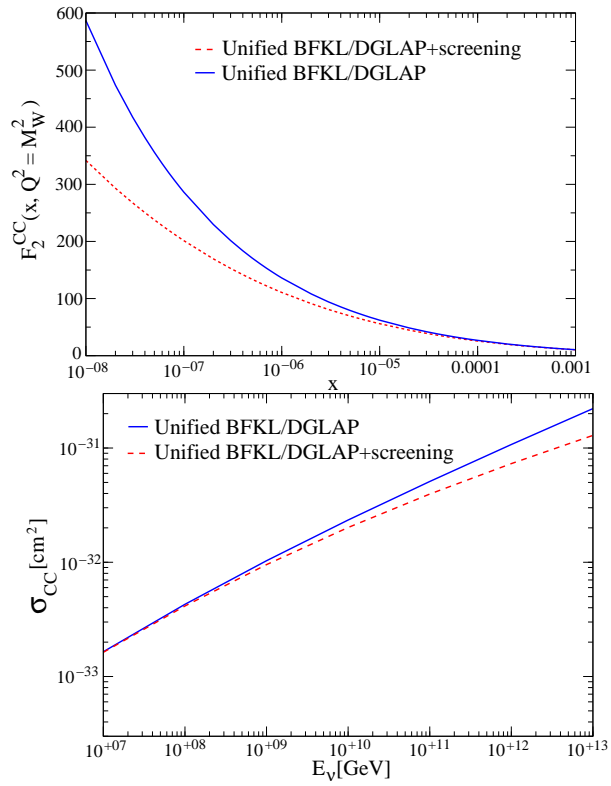


Fig. 8: (left) Charged current $F_2^{CC}(x, Q^2)$ structure function , (right) neutrino cross-section obtained from BK (with subleading corrections) and from BFKL (with subleading corrections)

- [12] R. Engel and H. Rebel, *Acta Phys. Polon.* **B35**, 321 (2004).
- [13] C. Meurer, J. Bluemer, R. Engel, A. Haungs, and M. Roth, *Czech. J. Phys.* **56**, A211 (2006), [arXiv:astro-ph/0512536](https://arxiv.org/abs/astro-ph/0512536).
- [14] Particle Data Group Collaboration, C. Caso *et al.*, *Eur. Phys. J.* **C3**, 1 (1998).
- [15] H. H. Mielke, M. Foeller, J. Engler, and J. Knapp, *J. Phys.* **G20**, 637 (1994);
G. b. Yodh, S. c. Tonwar, T. k. Gaisser, and R. w. Ellsworth, *Phys. Rev.* **D27**, 1183 (1983);
M. Honda *et al.*, *Phys. Rev. Lett.* **70**, 525 (1993);
R. M. Baltrusaitis *et al.*, *Phys. Rev. Lett.* **52**, 1380 (1984).
- [16] UA5 Collaboration, R. E. Ansorge *et al.*, *Z. Phys.* **C43**, 357 (1989).
- [17] A. Bunyatyan *et al.*, *Experimental results (see fig 6)*. These proceedings.
- [18] ZEUS Collaboration, S. C. e. a. ZEUS Coll., *Nucl. Phys.* **B658**, 3 (2003), [arXiv:hep-ex/0210029](https://arxiv.org/abs/hep-ex/0210029).
- [19] A. Bunyatyan *et al.*, *Experimental results*. These proceedings.
- [20] T. Pierog and K. Werner, *Phys. Rev. Lett.* **101**, 171101 (2008), [arXiv:astro-ph/0611311](https://arxiv.org/abs/astro-ph/0611311).
- [21] NA49 Collaboration, T. Susa, *Nucl. Phys.* **A698**, 491 (2002).
- [22] E735 Collaboration, T. Alexopoulos *et al.*, *Phys. Rev.* **D48**, 984 (1993).
- [23] V. N. Gribov, *Sov. Phys. JETP* **26**, 414 (1968);
V. N. Gribov, *Sov. Phys. JETP* **29**, 483 (1969).
- [24] V. A. Abramovsky, V. N. Gribov, and O. V. Kancheli, *Yad. Fiz.* **18**, 595 (1973).
- [25] A. B. Kaidalov, *Phys. Rept.* **50**, 157 (1979).
- [26] J. L. Cardy, *Nucl. Phys.* **B75**, 413 (1974);
A. B. Kaidalov, L. A. Ponomarev, and K. A. Ter-Martirosian, *Yad. Fiz.* **44**, 722 (1986).
- [27] S. Ostapchenko, *Phys. Rev.* **D77**, 034009 (2008), [arXiv:hep-ph/0612175](https://arxiv.org/abs/hep-ph/0612175).
- [28] L. Durand and P. Hong, *Phys. Rev. Lett.* **58**, 303 (1987);
X.-N. Wang, *Phys. Rept.* **280**, 287 (1997), [arXiv:hep-ph/9605214](https://arxiv.org/abs/hep-ph/9605214);
F. M. Liu, H. J. Drescher, S. Ostapchenko, T. Pierog, and K. Werner, *J. Phys.* **G28**, 2597 (2002), [arXiv:hep-ph/0109104](https://arxiv.org/abs/hep-ph/0109104).
- [29] F. W. Bopp, R. Engel, D. Pertermann, and J. Ranft, *Phys. Rev.* **D49**, 3236 (1994).
- [30] T. C. Rogers, A. M. Stasto, and M. I. Strikman, *Phys. Rev.* **D77**, 114009 (2008), [arXiv:0801.0303 \[hep-ph\]](https://arxiv.org/abs/0801.0303).
- [31] L. V. Gribov, E. M. Levin, and M. G. Ryskin, *Phys. Rept.* **100**, 1 (1983).

- [32] J. Jalilian-Marian, A. Kovner, A. Leonidov, and H. Weigert, Nucl. Phys. **B504**, 415 (1997), [arXiv:hep-ph/9701284](#);
E. Iancu, A. Leonidov, and L. D. McLerran, Nucl. Phys. **A692**, 583 (2001),
[arXiv:hep-ph/0011241](#).
- [33] L. Frankfurt, M. Strikman, and C. Weiss, Ann. Rev. Nucl. Part. Sci. **55**, 403 (2005),
[arXiv:hep-ph/0507286](#).
- [34] L. Frankfurt, V. Guzey, M. McDermott, and M. Strikman, Phys. Rev. Lett. **87**, 192301 (2001), [arXiv:hep-ph/0104154](#).
- [35] L. Frankfurt and M. Strikman, Phys. Lett. **B645**, 412 (2007).
- [36] A. Dumitru, L. Gerland, and M. Strikman, Phys. Rev. Lett. **90**, 092301 (2003),
[arXiv:hep-ph/0211324](#).
- [37] A. Berera, M. Strikman, W. S. Toothacker, W. D. Walker, and J. J. Whitmore, Phys. Lett. **B403**, 1 (1997), [arXiv:hep-ph/9604299](#).
- [38] F. Gelis, A. M. Stasto, and R. Venugopalan, Eur. Phys. J. **C48**, 489 (2006),
[arXiv:hep-ph/0605087](#).
- [39] H. J. Drescher and M. Strikman, Phys. Rev. Lett. **100**, 152002 (2008).
- [40] K. Hencken *et al.*, Phys. Rept. **458**, 1 (2008), [arXiv:0706.3356 \[nucl-ex\]](#).
- [41] R. A. Vazquez, Nucl. Phys. Proc. Suppl. **175-176**, 487 (2008).
- [42] S. Klein, Rev. Mod. Phys. **71**, 1501 (1999), [arXiv:hep-ph/9802442](#).
- [43] T. C. Rogers and M. I. Strikman, J. Phys. **G32**, 2041 (2006),
[arXiv:hep-ph/0512311](#).
- [44] V. N. Gribov, Zh. Eksp. Teor. Fiz. **57**, 1306 (1969). SLAC-TRANS-0102;
L. B. Bezrukov and E. V. Bugaev, Yad. Fiz. **33**, 1195 (1981);
E. Gotsman, E. M. Levin, and U. Maor, Eur. Phys. J. **C5**, 303 (1998),
[arXiv:hep-ph/9708275](#).
- [45] A. Donnachie and P. V. Landshoff, Phys. Lett. **B518**, 63 (2001),
[arXiv:hep-ph/0105088](#).
- [46] E. V. Bugaev, Nucl. Phys. Proc. Suppl. **175-176**, 117 (2008).
- [47] M. McDermott, L. Frankfurt, V. Guzey, and M. Strikman, Eur. Phys. J. **C16**, 641 (2000),
[arXiv:hep-ph/9912547](#).
- [48] M. M. Block and F. Halzen, Phys. Rev. **D70**, 091901 (2004),
[arXiv:hep-ph/0405174](#).

- [49] V. P. Goncalves and M. V. T. Machado, JHEP **04**, 028 (2007),
arXiv:hep-ph/0607125.
- [50] I. Balitsky, Nucl. Phys. **B463**, 99 (1996), arXiv:hep-ph/9509348;
Y. V. Kovchegov, Phys. Rev. **D60**, 034008 (1999), arXiv:hep-ph/9901281.
- [51] E. A. Kuraev, L. N. Lipatov, and V. S. Fadin, Sov. Phys. JETP **45**, 199 (1977).
- [52] K. Kutak and J. Kwiecinski, Eur. Phys. J. **C29**, 521 (2003), arXiv:hep-ph/0303209.